Journal of Mathematical Chemistry Vol. 38, No. 3, October 2005 (© 2005)
DOI: 10.1007/s10910-005-5823-8

An application of mean-field perturbation theory for the adsorption of polar molecules in nanoslit-pores

Rasesh R. Kotdawala, Nikolaos Kazantzis,* and Robert W. Thompson
Department of Chemical Engineering, Worcester Polytechnic Institute, Worcester, MA 01609, USA
E-mail: nikolas@wpi.edu

Received 2 March 2005; revised 22 March 2005

In the present research study, we present the development of a model for characterizing and predicting the adsorption of polar molecules between two parallel plates based on mean-field perturbation theory. The electrostatic forces between fluid–fluid molecules in the slit shaped pore are modeled by considering permanent dipole–dipole interactions and permanent dipole-induced dipole moment interactions. The intermolecular potential for the electrostatic interactions was obtained by considering statistical averages over all possible orientations of the molecules. The proposed model is then used to study the sorption of water molecules in the slit shaped pore and an explicit equation for the Helmholtz free energy of the pore phase fluid is derived. Adsorption isotherms for different pore sizes are simulated and the relative contributions of fluid–wall and fluid–fluid interactions to the Helmholtz free energy are calculated as an illustration and compared with the results of existing models in the literature.

KEY WORDS: statistical mechanics, perturbation theory, averaging methods, adsorption modeling, nanopores

AMS subject classification: 82B03, 82B05, 82B26, 82B30, 82D15, 31B10, 41A25

1. Introduction

One of the most successful approaches to the study of liquids in recent years relied on the development of perturbation theories. Their essential physical basis is the separation of the roles of attractive and repulsive intermolecular forces. It is proposed that the structure of simple liquids, as revealed by their radial distribution functions (RDFs), is chiefly determined by the packing requirements of the molecules, which in turn reflects the repulsive intermolecular forces [1–4]. The attractive forces are thought to serve essentially as the "glue" that holds molecules together, maintaining the high density, but otherwise playing no major structural role [1–4]. When the structures of hard sphere liquids are compared with those of real monatomic liquids, close similarities are seen

*Corresponding author.

[1–4]. This suggests that the effects of the soft repulsive forces of real molecules may be modeled with reasonable accuracy using a hard-sphere system. Notice that the properties of hard-sphere systems are well known from computer simulations as well as from statistical mechanical theories [1–4]. Furthermore, in the formal development of perturbation theories, the effects of changes in the form of the intermolecular potential on the properties of a system of molecules can be studied in a transparent manner [1–4]. For pair wise–additive systems the pair potential energy function is the sum of the reference potential, $U_0(r)$, and the perturbation potential, $U_1(r)$ [1]:

$$U(r) = U_0(r) + U_1(r). \tag{1}$$

The properties of the system of molecules interacting through $U_0(r)$ are assumed to be known, and those of the perturbed system are expressed in terms of $U_1(r)$ and the properties of the reference system. For example, the configuration energy, U_N, for a system of N molecules interacting through $U(r)$ may be written (to first order in classical perturbation theory) as follows [1]:

$$U_N = U_N^0 + \frac{N^2}{2V}\int_0^\infty 4\pi r^2 g^0(r) U_1(r)\mathrm{d}r, \tag{2}$$

where U_N^0 is the configuration energy of the reference system whose RDF is $g^0(r)$, and V is the volume of the system. Similar expressions for other properties may also be written, and these are also quite easily calculated if $g^0(r)$ is known [1]. Higher-order perturbation terms may also be added, but their calculation is much more demanding, and the successful application of this theory depends on the rapid convergence of the expansion [1]. This, in turn, will depend on the choice of a reference system whose structure faithfully mimics that of the system under study [1–4]. The success of this approach has thus rested on the correct choice of the division of $U(r)$ into reference and perturbation potentials [1]. Notice, that the results of the first-order perturbation theory are found to be sensitive to the choice of the hard-sphere diameter d [1]. Barker and Henderson (described in [1–4]) considered the effect of temperature but not of density in the proposed perturbation theory. They were able to calculate the first-order and second-order perturbation terms, using computer simulation results. Furthermore, calculations of the properties of Lennard–Jones liquids were found to be in very good agreement with those obtained from direct computer simulation [1–4]. The second-order term, though small, was found to be necessary to achieve an excellent level of agreement. Week, Chandler, and Anderson have proposed a perturbation theory based on a novel choice of reference and perturbation potentials [1]. They assigned the whole repulsive region of $U(r)$ to the role of the reference potential and determinant of the structure, rather than just the positive portion of $U(r)$, as in the aforementioned Baker–Henderson theory. A consequence of

this division is that the perturbation energy $U_1(r)$ is now a very smoothly varying function of r, and this has the useful effect of reducing the higher-order fluctuation terms, thus giving a very accurate equation of state even when restricted to a first- order treatment [1,2,4]. Due to their ability to predict liquid properties, perturbation theories seem to be attractive to study gas–liquid phase transitions in micro porous materials, especially to study the behavior of fluid molecules in nano materials and sorption in micro porous materials [1,2,4].

Several efforts have been made to simulate adsorption isotherms and isosteric heats of adsorption using density functional and mean field theories for non-polar compounds like Leonard–Jones fluids for both slit and cylindrical shaped pores [5–9]. For the adsorption of polar compounds the general approach is to use Monte–Carlo techniques, because of the presence of angle-dependent electrostatic interactions [10,11]. However, Truskett et al. [12,13] and Giaya and Thompson [14,15] proposed an analytical treatment of partition functions for the water–slit pore system by including a hydrogen bonding term and by extending the model originally proposed by Schoen and Diestler [5]. However, their approach requires the exact analytical expressions of RDFs at different densities and temperatures, which are not available in the literature for some polar molecules. In order to overcome the difficulty of integrating the intermolecular potential over all possible orientations of molecules, we use in the present study, the method of averaging the orientation-dependent electrostatic intermolecular potential terms over all possible molecular orientations in a spirit similar to the one in [3]. In particular, the approximate intermolecular potential function that is derived by statistical averaging is used in the context of the proposed mean-field perturbation theoretical model presented here, and the electrostatic interactions are explicitly computed. The model developed in the present study is then used to predict the sorption of water confined in nanoslit-pores.

The paper is organized as follows. Section 2 introduces the proposed mean-field perturbation approach and statistical averaging method associated with the electrostatic molecular potential. In section 3, the resulting statistical-mechanical model's prediction of the adsorption isotherms, as well as isosteric heat of adsorption of water molecules adsorbed in a nanoslit-pore domain are compared with available results in the literature and the proposed method's advantages/limitations discussed.

2. Model development

Consider the fluid confined in the slit shaped pore of s_z width shown in figure 1.

From previous work [5,12–15] the Helmholtz free energy for the fluid confined between two parallel plates is given by

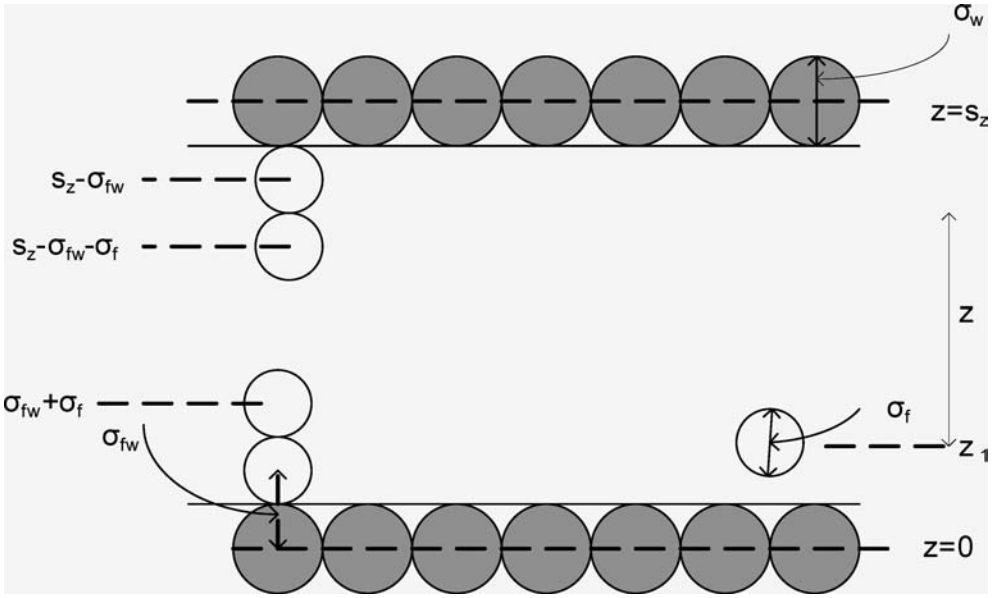

Figure 1. Side view of the slit pore model showing wall atoms and fluid molecules.

$$F = -\beta^{-1} \ln \left(\frac{Z_N^{(0)}}{N! \lambda^{3N}} \right) + \langle U^{(1)} \rangle_0, \tag{3}$$

where, $\langle U^{(1)} \rangle_0 = \langle u_{ff}(r) \rangle + \langle u_{fw}(z_i) \rangle$, $\beta = 1/\mathrm{kT}$ is a Boltzmann factor, λ is the thermal wave length, $Z^{(0)}$ is the configuration partition function for a confined hard sphere fluid, (it is typically referred to as the configuration integral of the reference system) and $\langle u_{ff}(r) \rangle$ and $\langle u_{fw}(z_i) \rangle$ are average potential energies associated with the fluid–wall and fluid–fluid (electrostatic + dispersion) interactions, respectively. Collectively, they are also called as the energy of the perturbation from the reference system ($\langle U^{(1)} \rangle_0$).

2.1. Energy of the reference system

A hard sphere fluid confined in a hard sphere slit shaped pore is considered as a reference system, in analogy with previous work [5,12–15]. Moreover, the wall is considered to be smooth, that is, ignoring local variations on the wall surface. First, we define the potential energy of the reference system $U^{(0)}$ as follows:

$$U^{(0)} = \frac{1}{2} \sum_{i=1}^{N} \sum_{j \neq 1}^{N} u_{hs,ff}(r_{ij}) + \sum_{i=1}^{N} u_{hs,fw}(z_i), \tag{4}$$

where the fluid–fluid interaction potential term of the hard sphere system is defined as follows:

$$u_{hs,ff}(r_{ij}) = \begin{cases} 0, & r_{ij} > \sigma_f, \\ \infty & r_{ij} \leqslant \sigma_f \end{cases} \tag{5}$$

and the fluid–wall interaction potential term through the following expression:

$$u_{hs,fw}(z_i) = \begin{cases} 0, & \sigma_{fw} < z_i < s_z - \sigma_{fw}, \\ \infty & z_i \leqslant \sigma_{fw} \ or \ z_i \geqslant s_z - \sigma_{fw}. \end{cases} \tag{6}$$

In equation (5) $r_{ij} \equiv \|r_i - r_j\|$ is the distance between a pair of hard spheres with centers located at r_i and r_j, $\sigma_{fw} = (\sigma_f + \sigma_w)/2$ is the distance between a fluid molecule and a substrate atom in contact, and s_z is the distance between the walls of the pore (see figure 1). The configuration integral of the reference system ($Z_N^{(0)}$) can be approximated by $(Z_1^{(0)})^N$, where, $Z_1^{(0)}$ is the effective single-molecule configuration integral [2, 5]. We take $Z_1^{(0)}$ to be equal to the volume accessible to any given molecule: $A(s_z - 2\sigma_{fw}) - Nb$, where A is the area of the wall and $b = 2\pi\sigma_{fw}^3/3$ is the volume excluded to one molecule by another [2, 5]. Hence, the reference system is thermodynamically characterized by:

$$Z_N^{(0)} = (A(s_z - 2\sigma_{fw}) - Nb)^N. \tag{7}$$

2.2. *Energy of the perturbation*

The perturbation potential term is similarly given by the following expression:

$$U^{(1)} = \frac{1}{2}\sum_{i=1}^{N}\sum_{j\neq i}^{N} u_{ff}(r_{ij}) + \sum_{i=1}^{N} u_{fw}(z_i), \tag{8}$$

where $u_{ff}(r_{ij})$ is the total pair potential for fluid–fluid interactions which includes terms for the dispersion force interaction as well as the direct electrostatic energies. The following equation for the fluid–fluid interactions for polar molecules is used as developed in [16–18],

$$u_{ff}(r_{ij}) = \left[-\frac{1}{(4\pi\varepsilon_0)^2 r_{ij}^6} \left(\frac{3\alpha_i\alpha_j(I_i + I_j)}{I_i I_j 4} \right) \right] + \gamma, \tag{9}$$

where I_i and I_j is the first ionization potential for molecule i and j, respectively, ε_0 is the electric permittivity of vacuum, and α_i, α_j is the average polarizability of molecules i and j, respectively. The term γ accounts for the interactions due to permanent dipole moments between two molecules, as well as induced dipole and permanent dipole moments between the two molecules under consideration

[3]. $u_{fw}(z_i)$ is the fluid–wall intermolecular potential and is typically given by the following expression [5, 12–15]:

$$u_{fw}(z_i) = \frac{-2\pi\rho_w\varepsilon_{fw}\sigma_{fw}^6}{3d}\left[z_i^{-3} + (s_z - z_i)^{-3}\right], \quad \sigma_{fw} < z_i < s_z - \sigma_{fw}. \tag{10}$$

Here, $\varepsilon_{fw} = (\varepsilon_f\varepsilon_w)^{1/2}$, ρ_w is the aerial density of the solid substrate, and d is the distance between two wall atoms. $\varepsilon_{f,}\varepsilon_w$ and ε_{fw} are the fluid–fluid, wall–wall and fluid–wall interaction parameters, respectively.

Notice that the term γ is given by the following expression [3]:

$$\gamma = u_{\mu\mu} + u_{\mu\alpha}. \tag{11}$$

In particular:

$$u^{\mu\mu} = \frac{\mu_i\mu_j}{r_{ij}^3}g \tag{12}$$

with μ_i, μ_j being the permanent dipole moments associated with molecules i and j, respectively, and $g = \sin\theta_i \sin\theta_j \cos\phi_{ij} - 2\cos\theta_i \cos\theta_j$ (where, θ_i and θ_j are the angles between the molecular dipole moment vector and the line joining the center of the two molecules i and j, respectively, as shown in figure 2).

Furthermore, the following quantities are given by [3]:

$$u_{\mu\alpha} = \frac{-1}{r_{ij}^6}\left(\alpha_i\mu_j^2(3\cos^2\theta_j + 1) + \alpha_j\mu_i^2(3\cos^2\theta_i + 1)\right), \tag{13}$$

$$\gamma = -\frac{\mu_i\mu_j}{r_{ij}^3}g - \frac{1}{r_{ij}^6}\left(\alpha_i\mu_j^2(3\cos^2\theta_j + 1) + \alpha_j\mu_i^2(3\cos^2\theta_i + 1)\right). \tag{14}$$

2.3. *Statistical averaging for the dipole–dipole intermolecular potential*

The coordinate systems for two charge distributions representing molecules i and j are shown in figure 2. In particular, one specific relative orientation is shown and determined by the polar angles θ_i and θ_j, as well as the azimuthal angle φ_{ij} at a separation r_{ij}. Furthermore, we have chosen each z axis as the direction of the dipole-moment vector μ.

The configuration integral $Z_{\mu\mu}$ for the pair of molecules is given by [3]:

$$Z_{\mu\mu} = \frac{1}{16\pi^2}\int \ldots \int \mathrm{e}^{-\beta u_{\mu\mu}}\,\mathrm{d}r_i\,\mathrm{d}r_j\,\mathrm{d}\omega_i\,\mathrm{d}\omega_j, \tag{15}$$

where $\mathrm{d}\omega_i\,\mathrm{d}\omega_j = \sin\theta_i \sin\theta_j\,\mathrm{d}\theta_i\,\mathrm{d}\theta_j\,\mathrm{d}\phi_i\,\mathrm{d}\phi_j$. Using the relative coordinates $r = r_i - r_j$ and $\phi_{ij} = \phi_i - \phi_j$, the configuration-space volume element can be written as: $\mathrm{d}r_i\,\mathrm{d}r_j\,\mathrm{d}\omega_i\,\mathrm{d}\omega_j = \mathrm{d}r_i\,\mathrm{d}r\,\sin\theta_i \sin\theta_j\,\mathrm{d}\theta_i\,\mathrm{d}\theta_j\,\mathrm{d}\phi_i\,\mathrm{d}\phi_{ij}$.

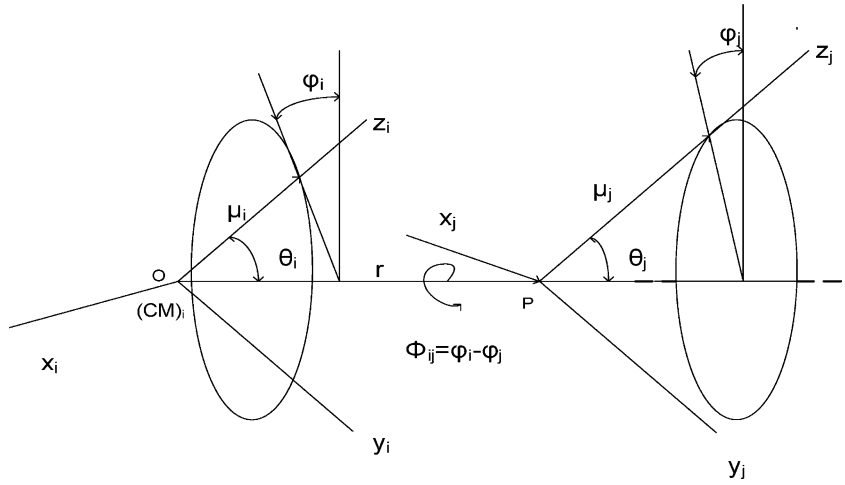

Figure 2. Two static charge systems with z axes in the direction of the dipole moments and separated by distance r between the centers of mass [3].

Notice that the multiple integrals in $Z_{\mu\mu}$ over $\mathrm{d}r_i$ and $\mathrm{d}\phi_i$ give V and 2π, respectively, and therefore:

$$Z_{\mu\mu} = \frac{V}{8\pi} \int \int \mathrm{e}^{-\beta u_{\mu\mu}} \mathrm{d}r \, \mathrm{d}\omega, \tag{16}$$

where $\mathrm{d}\omega = \sin\theta_i \sin\theta_j \, \mathrm{d}\theta_i \, \mathrm{d}\theta_j \, \mathrm{d}\phi_{ij}$.

Let $\varsigma_{\mu\mu}$ be the phase integral for the angular coordinates of a pair of molecules:

$$\varsigma_{\mu\mu} = \frac{1}{8\pi} \int \mathrm{e}^{-\beta u_{\mu\mu}} \mathrm{d}\omega. \tag{17}$$

If we now define a function by $\varsigma_{\mathrm{e}} \equiv \mathrm{e}^{-\beta\gamma_1}$, where γ_1 is an angle-averaged energy function, we can replace an angle-dependent pair-potential energy function $u_{\mu\mu}(r, \theta_i, \theta_j, \theta_{ij})$ by the angle-independent function $u_{\mu\mu}(r, T)$. Indeed, equation (16) can be written as follows:

$$Z_{\mu\mu} = V \int \mathrm{e}^{-\beta\gamma_1} \mathrm{d}r. \tag{18}$$

Note that $\varsigma_{\mu\mu}$ and γ_1 are functions of r and T. The term $\mathrm{e}^{-\beta\gamma_1}$ plays the role of an apparent Boltzmann factor. Furthermore, γ_1 is actually a Helmholtz free energy term of orientation for the molecular pair. From its definition γ_1 is calculated by:

$$\gamma_1 = -\frac{1}{\beta} \ln \varsigma_{\mu\mu} = -kT \ln \left(\frac{1}{8\pi} \int \mathrm{e}^{-\beta u_{\mu\mu}} \mathrm{d}\omega \right), \tag{19}$$

where,

$$u^{\mu\mu} = \frac{\mu_i \mu_j}{r_{ij}^3} g \tag{20}$$

and $g = \sin\theta_i \sin\theta_j \cos\phi_{ij} - 2\cos\theta_i \cos\theta_j$.

It can be shown that when the temperature is not too low, for example, $T > 100\,\mathrm{K}$ for $\mu \leqslant 2D$ or $T > 200\,\mathrm{K}$ for $\mu \leqslant 3D$, the infinite series expansion of the above exponential function converges rapidly and hence [3]:

$$\varsigma_{\mu\mu} = \frac{1}{8\pi} \int \left(1 - \frac{\mu_i \mu_j}{r_{ij}^3} \beta g + \frac{\mu_i^2 \mu_j^2}{2 r_{ij}^6} \beta^2 g^2 - \cdots\right) \mathrm{d}\omega. \tag{21}$$

The integration is over the three variables present in g, namely: $\theta_a \in [0, \pi]$, $\theta_b \in [0, \pi]$, and $\phi_{ij} \in [0, 2\pi]$. The following integration results hold true:

$$\int \mathrm{d}\omega = 8\pi \quad \int g\,\mathrm{d}\omega = 0 \quad \int g^2\,\mathrm{d}\omega = \frac{16}{3}\pi \quad \int g^3\,\mathrm{d}\omega = 0.$$

In the light of the above integration results, a term by term integration of the uniformly convergent series in equation (21) yields:

$$\varsigma_{\mu\mu} = 1 + \frac{\mu_i^2 \mu_j^2 \beta^2}{3 r_{ij}^6} + \cdots \tag{22}$$

Note that γ, the free energy averaged potential for dipole–dipole interactions, can be obtained by substituting equation (22) into (19):

$$\gamma_1 = -kT \ln\left(1 + \frac{\mu_i^2 \mu_j^2 \beta^2}{3 r_{ij}^6} + \cdots\right) \tag{23}$$

which can be further approximated as follows:

$$\gamma_1 = u_{\mu\mu} \approx -\frac{\mu_i^2 \mu_j^2}{3kT r_{ij}^6}, \tag{24}$$

whenever the argument$|\mu_i \mu_j / kT r_{ij}^3| \ll 1$, namely in a regime where $T > 300\,\mathrm{K}$ and μ_i, $\mu_j < 3\mathrm{D}$.

2.4. Dipole–induced dipole moment interactions

Let us now consider the potential term associated with the dipole-induced dipole moment interactions:

$$u_{\mu\alpha} = \frac{-1}{r_{ij}^6}\left(\alpha_i\mu_j^2(3\cos^2\theta_j + 1) + \alpha_j\mu_i^2(3\cos^2\theta_i + 1)\right). \tag{25}$$

After carrying out the aforementioned statistical averaging method, in a similar way as before, one obtains an expression for the corresponding energy terms. In particular, one obtains:

$$u_{\mu\alpha} \approx -\left(\frac{\mu_i^2\alpha_j - \mu_j^2\alpha_i}{r_{ij}^6}\right). \tag{26}$$

Combining equations (11), (24) and (26) the following equation can be derived:

$$\gamma = -\frac{\mu_i^2\mu_j^2}{3kTr_{ij}^6} - \frac{\mu_i^2\alpha_j}{r_{ij}^6} - \frac{\mu_j^2\alpha_i}{r_{ij}^6}, \tag{27}$$

where, μ_i, μ_j are the permanent dipole moments associated with molecule i and molecule j, and α_i, α_j is the respective average polarizability. For the same kind of molecule $i = j$, (dropping subscripts and combining equations (9) and (27)), we have:

$$u_{ff}(r) = \left[-\frac{1}{(4\pi\varepsilon_0)^2r^6}\left(\frac{3\alpha^2I}{4}\right)\right] - \frac{1}{r^6}\left(\frac{\mu^4}{3kT} + 2\mu^2\alpha\right). \tag{28}$$

Note that [5,12–15]:

$$\langle u_{ff}(r)\rangle = \frac{1}{2}\int_V \mathrm{d}r_1 \int_V \mathrm{d}r_2 g(r_1, r_2)\rho_0^{(1)}(r_1)\rho_0^{(1)}(r_2)u_{a,ff}(r_{ij}). \tag{29}$$

We now seek an equation of state under the mean-field assumption, ignoring intermolecular correlations and setting [5,12–15]:

$$g(r_1, r_2) = \begin{cases} 0, & r_{12} < \sigma_f, \\ 1, & r_{12} \geqslant \sigma_f, \end{cases} \tag{30}$$

Furthermore, assuming that the fluid of interest is homogeneous throughout the pore volume, we can approximate the local density by [5,12–15]:

$$\rho_0^{(1)}(r_1) = \rho_0^{(1)}(r_2) = \rho_p = \frac{N}{A(s_z - 2\sigma_{fw})}. \tag{31}$$

Using the approximations in equations (30) and (31), the volume integral in equation (29) can be readily simplified and become an one-dimensional integral.

By substituting equation (28) into (29) and transforming the integration variables in the double integral in equation (29) from $\{r_1, r_2\}$ to $\{r_1, r_{12}\}$, we have:

$$\langle u_{ff}(r)\rangle = \frac{a_{p1}}{A(s_z - 2\sigma_{fw})}\int_V \mathrm{d}r_1 \int_V \mathrm{d}r_{12} g(r_{12}) r_{12}^{-6} \tag{32}$$

$$= \frac{a_{p1}}{(s_z - 2\sigma_{fw})}\int_{\sigma_{fw}}^{s_z-\sigma_{fw}} \mathrm{d}z_1 \int_{\bar{V}(z_1)} \mathrm{d}r_{12} r_{12}^{-6} \tag{33}$$

$$= \frac{2\pi a_{p1}}{(s_z - 2\sigma_{fw})}\int_{\sigma_{fw}}^{s_z-\sigma_{fw}} \mathrm{d}z_1 \left\{\int \mathrm{d}z \int \mathrm{d}\rho\rho (z^2+\rho^2)^{-3}\right\}_{\bar{V}(z_1)}, \tag{34}$$

where

$$a_{p1} = \frac{1}{(4\pi\varepsilon_0)^2}\left[\left(\frac{2\mu^4}{3kT}\right) + 2\mu^2\alpha + \left(\frac{3\alpha^2 I}{4}\right)\right] \tag{35}$$

and $\bar{V}_{(z_1)}$ denotes the z_1-dependent volume restricted by hard cores of fluid molecules and by the hard walls. Note that, for $s_z > 2(\sigma_{fw} + \sigma_f)$, the integration on z_1 breaks down into three ranges: (1) $\sigma_{fw} < z_1 < \sigma_f$, (2) $\sigma_{fw} + \sigma_f < z_1 < s_z - (\sigma_{fw} + \sigma_f)$, and (3) $s_z - (\sigma_{fw} + \sigma_f) < z_1 < s_z - \sigma_{fw}$. [5].

In turn, the integrations on z and ρ can be broken into either two or three regions within each range of z_1.Thus $\langle u_{ff}(r)\rangle$ splits into three contributions $\langle u_{ff}(r)\rangle = a_1 + a_2 + a_3$. First note that, by symmetry $a_1 = a_3$

For a_1, one obtains:

$$a_1 = a_3 = \frac{2\pi a_{p1}}{(s_z - 2\sigma_{fw})}\int_{\sigma_{fw}}^{\sigma_{fw}+\sigma_f} \mathrm{d}z_1$$

$$\times \left\{\int_{-z_1+\sigma_{fw}}^{\sigma_f} \mathrm{d}z \int_{\sqrt{\sigma_f^2 - z^2}}^{\infty} \frac{\mathrm{d}\rho\rho}{(z^2+\rho^2)^3} + \int_{\sigma_f}^{s_z-\sigma_{fw}-z_1} \mathrm{d}z \int_0^{\infty} \frac{\mathrm{d}\rho\rho}{(z^2+\rho^2)^3}\right\} \tag{36}$$

$$= \frac{2\pi a_{p1}}{(s_z - 2\sigma_{fw})}\left\{\frac{11}{24\sigma_f^2} - \frac{1}{24}\left[\frac{1}{(s_z - 2\sigma_{fw} - \sigma_f)^2} - \frac{1}{(s_z - 2\sigma_{fw})^2}\right]\right\}. \tag{37}$$

In a similar fashion we obtain,

$$a_2 = \frac{2\pi a_{p1}}{(s_z - 2\sigma_{fw})} \int_{\sigma_{fw}+\sigma_f}^{s_z-\sigma_{fw}-\sigma_f} \mathrm{d}z_1 \left\{ \int_{-z_1+\sigma_{fw}}^{-\sigma_f} \mathrm{d}z \int_0^\infty \frac{\mathrm{d}\rho\rho}{(z^2+\rho^2)^3} + \int_{-\sigma_f}^{\sigma_f} \mathrm{d}z \int_{\sqrt{\sigma_f^2-z^2}}^\infty \frac{\mathrm{d}\rho\rho}{(z^2+\rho^2)^2} + \int_{\sigma_f}^{s_z-z_1-\sigma_{fw}} \mathrm{d}z \int_0^\infty \frac{\mathrm{d}\rho\rho}{(z^2+\rho^2)^3} \right\} \quad (38)$$

$$= \frac{4\pi a_{p1}}{(s_z - 2\sigma_{fw})} \left\{ \frac{1}{3\sigma_f^3}[s_z - 2\sigma_{fw} - 2\sigma_f] + \frac{1}{24}\left[\frac{1}{(s_z - 2\sigma_{fw} - \sigma_f)^2} - \frac{1}{\sigma_f^2} \right] \right\}. \quad (39)$$

Combining equations (36), (39), and (29) yields:

$$\langle u_{ff}(r) \rangle = -2a_p \rho_p N, \quad (40)$$

where:

$$a_p = \frac{4\pi a_{p1}}{3\sigma_f^3 (s_z - 2\sigma_{fw})} \left[-\frac{3}{2}\sigma_f + 2(s_z - 2\sigma_{fw}) + \frac{\sigma_f^3}{4(s_z - 2\sigma_{fw})^2} \right]. \quad (41)$$

2.5. Fluid–wall interactions

Consider equation (10) for the potential term associated with the fluid–wall interactions. The average fluid–wall interactions can be given by the following integral [5,12–15]:

$$\langle u_{fw}(z_i) \rangle = \int_V \mathrm{d}r_1 \rho_0^{(1)}(r_1) u_{a,fw}(z_1). \quad (42)$$

One can approximate the integral in (42) using (31) as follows:

$$\langle u_{fw}(z_i) \rangle = \frac{2\pi \rho_w \varepsilon_{fw} \sigma_{fw}^6 \rho_p A}{3d} \int_{\sigma_{fw}}^{sz-\sigma_{fw}} \left[z_i^{-3} + (sz - z_i)^{-3} \right] \mathrm{d}z \quad (43)$$

$$= \frac{2\pi \rho_w \varepsilon_{fw} \sigma_{fw}^6 \rho_p A}{3d} \left(\frac{s_z(s_z - 2\sigma_{fw})}{(s_z - \sigma_{fw})^2 \sigma_{fw}^2} \right), \quad (44)$$

$$\langle u_{fw}(z_i) \rangle = \psi(\xi) = \frac{2N\pi \rho_w \varepsilon_{fw} \sigma_{fw}^3}{3d(\xi - 2)} \left[\frac{1}{(\xi - 1)^2} - 1 \right], \xi > 2, \quad (45)$$

where, $\xi = \dfrac{s_z}{\sigma_{fw}}$.

Note that equations (8)–(13) now yield

$$\langle U^{(1)}\rangle_0 = \langle u_{ff}(r)\rangle + \langle u_{fw}(z_i)\rangle, \tag{46}$$

$$\langle U^{(1)}\rangle_0 = \psi(\xi)N - 2Na_p\rho_p. \tag{47}$$

Finally, substituting equations (7) and (47) into equation (3), one obtains the following expression for the Helmholtz free energy:

$$F = -\beta^{-1}\left\{N\ln\left[\frac{1-b\rho_p}{\rho_p\lambda^3}\right] + N\right\} + N\psi(\xi) - 2a_pN\rho_p. \tag{48}$$

2.6. Determination of equilibrium pore density

At equilibrium the following equation must be satisfied:

$$\mu_b(T, \rho_b) - \mu_P(T, \rho_P) = 0, \tag{49}$$

where $\mu_b(T, \rho_b)$ and $\mu_P(T, \rho_P)$ are the chemical potential for the bulk phase and the pore phase respectively. They can be calculated using equation (48) for the Helmholtz free energy as follows:

$$\mu_P(T, \rho_P) = \left(\frac{\partial F}{\partial N}\right)_{T,A,s_z} = \beta^{-1}\ln\left(\frac{\lambda^3\rho_P}{1-b\rho_p}\right) + \frac{\beta^{-1}b\rho_p}{1-b\rho_P} + \psi(\xi) - 2a_P(\xi)\rho_P, \tag{50}$$

$$\mu_b(T, \rho_b) = \lim_{\xi\to 0}\mu_P(T, \rho_P) = \beta^{-1}\ln\left(\frac{\lambda^3\rho_b}{1-b\rho_b}\right) + \frac{\beta^{-1}b\rho_b}{1-b\rho_b} - 2a_b\rho_b, \tag{51}$$

where

$$a_b = \frac{4\pi a_{p1}}{3\sigma_f^3}. \tag{52}$$

Equation (49) is a (non-linear) algebraic equation with unknown equilibrium pore density, keeping all other thermodynamic variables fixed. In the case of multiple real positive roots, the density value that minimizes the excess grand potential per unit wall area is typically selected, since it corresponds to the thermodynamically stable phase in the pores. It should be also emphasized (and will become clear in the next section) that the proposed statistical mechanics framework allows an insightful sensitivity analysis to be performed on the effect of parameters such as pore size and fluid–wall interaction parameter on the density of the confined phase and its thermodynamic stability. Furthermore, within

the context of the present study, issues pertaining to the structural characteristics of the corresponding liquid–vapor phase diagram as the above parameters vary can also be naturally addressed, since they are critically linked to any adsorbent design method.

3. Results and discussion

3.1. Pore filling

Figure 3(a) shows the adsorption isotherms at 298 K and a fixed value of the fluid–wall interaction parameter for different pore sizes. The vertical lines are drawn for guiding eyes. The pressure at which gas to liquid transition (pore filling) takes place decreases as the pore size decreases. Figure 3(b) shows the isotherms before the pore–filling takes place which are not seen clearly in figure 3(a). The pore density increases with decrease in pore sizes due to increased fluid–wall interactions. For 20, 25, and 30 Å pore sizes, the pore density after pore filling is close the density of liquid water, suggesting the capillary condensation takes place in the pores while in case of 15 and 18 Å pores the pore densities are between water vapor and liquid water. This can be explained by studying the magnitudes of the electrostatic interactions at different pore sizes.

The pore filling phenomena can be interpreted by studying the relative contributions of the fluid–fluid and fluid–wall interactions over the entire operating pressure range. The contributions as a function of operating bulk pressure are shown in figure 4 for 20 Å pores. The fluid–fluid interactions are split into two parts namely electrostatic and dispersion interactions. The results in figure 4 suggest that the fluid–wall interactions dominate over fluid–fluid interactions before pore filling takes place, but after pore filling by the liquid phase, the fluid–fluid interactions dominate due to strong electrostatic interactions attributed to the polar nature of water molecules.

The relative contributions of fluid–fluid and fluid–wall interactions at different pore sizes are shown in figure 5(a,b) at two different external pressures. figure 5(a) shows these values for conditions that result in capillary condensation of a liquid-like fluid. The results show that after pore filling the dispersion energy and the electrostatic energy increase with increase in the pore size. Figure 5(b) shows values for a vapor-like confined fluid. The results in figure 5(a) show that the electrostatic interaction energy increases as pore size increases, which is attributed to the orientation-dependent electrostatic interactions. The small pore size restricts the mobility of molecules in the pore, and hence the hydrogen bonds between water molecules get disrupted. Results in figure 5(b) show that as the monolayer forms the electrostatic and dispersion interactions increase

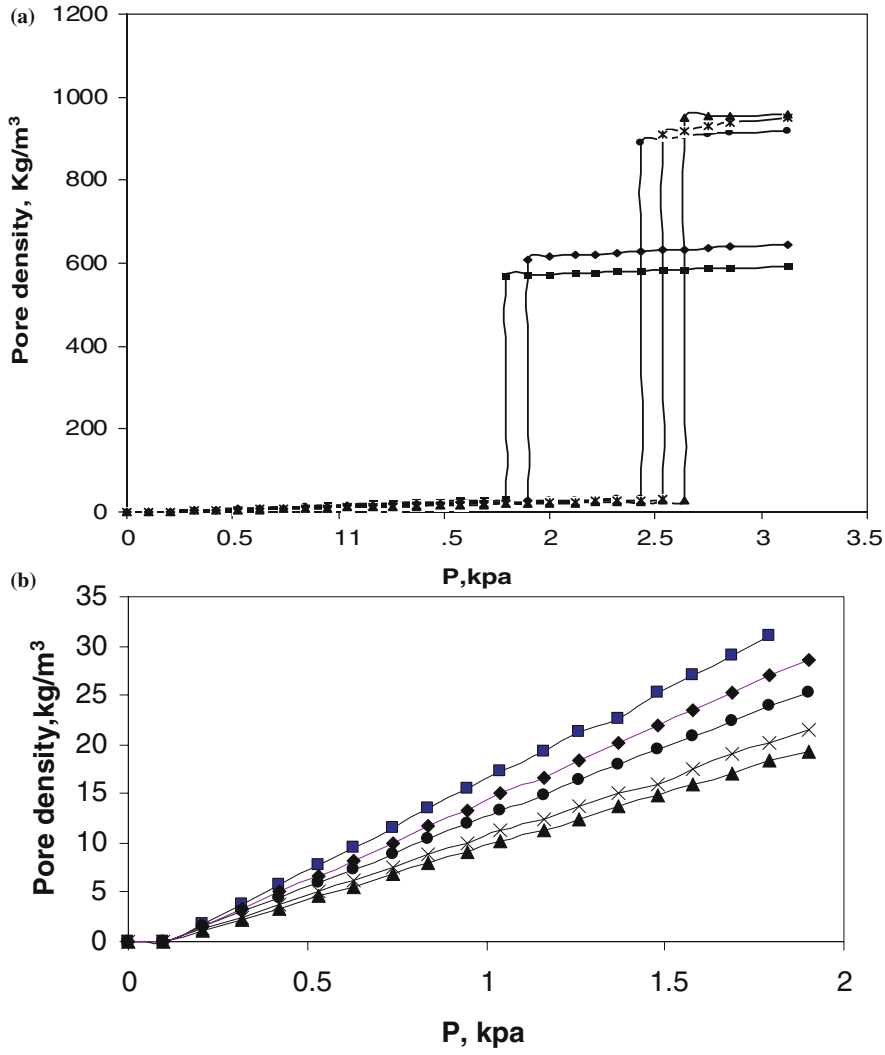

Figure 3. (a) Pore density of water molecules as a function of bulk pressure for water adsorbed in slit pores at 298 K and $\varepsilon_{fw} = 0.66$ kJ/mol. Results shown for pores of width 16 (■), 18 (♦), 20 (•), 25 (×) and 30 (▲) Å. (b) Pore densities of water molecules before pore filling by capillary condensation takes place at 298 K and $\varepsilon_{fw} = 0.66$ kJ/mol. Results shown for pores of width 16 (■), 18 (♦), 20 (•), 25 (×) and 30 (▲) Å.

with decrease in pore size due to neighboring molecules in the monolayer. This is attributed to an increase in the fluid–wall interactions which result in completion of monolayer formation at relatively low pressure.

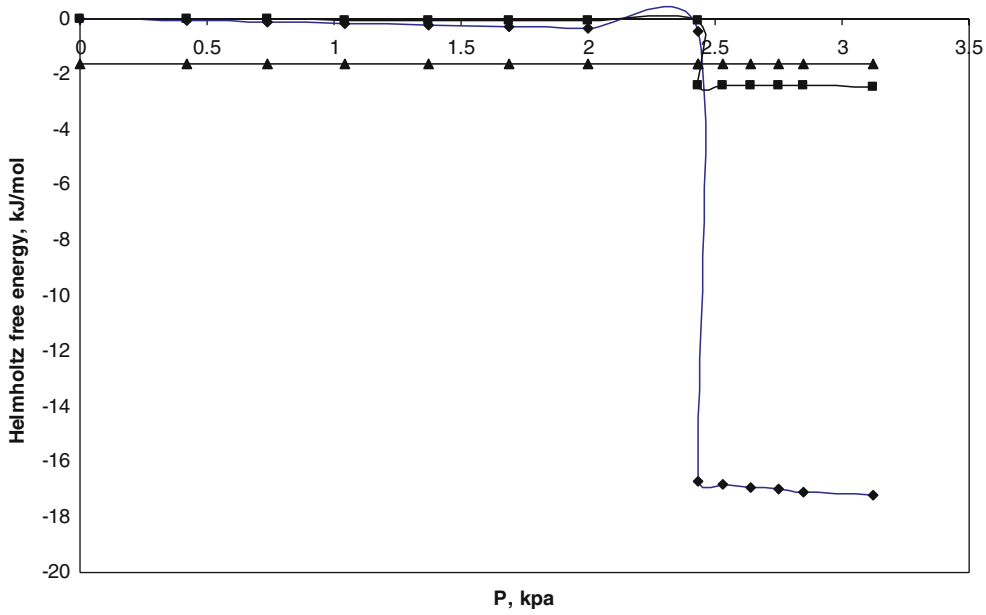

Figure 4. Relative magnitudes of the fluid–fluid electrostatic (♦), fluid–fluid dispersion (■), and fluid–wall interactions (▲). Helmholtz free energy as a function of bulk pressure for 20 Å pore width at 298 K and $\varepsilon_{fw} = 0.66$ kJ/mol.

3.2. Gas phase heat of adsorption

The isosteric heat of adsorption, q_{st}, is the heat released (per mole) on transferring an infinitesimally small amount of the adsorbate from the coexisting bulk gas phase to the adsorbed phase at constant temperature, pressure (constant adsorption loading), surface area A, and pore width H. As defined, q_{st}, can be related to entropies (S), internal energies (U), and volumes (V) of the two phases by Balbuena and Gubbins [8]:

$$q_{st} = T(S^{(g)} - S^{(a)}) = U^{(g)} - U^{(a)} + P(V^{(g)} - V^{(a)}), \tag{53}$$

where the subscripts (a) and (g) refer to the values for the adsorbed and bulk gas phases, respectively. The isosteric heat obeys the Clapeyron equation:

$$\left(\frac{\mathrm{d}P}{\mathrm{d}T}\right)_{A,s_z,\Gamma} = \frac{S^{(g)} - S^{(a)}}{V^{(g)} - V^{(a)}}, \tag{54}$$

where P is the pressure of the bulk gas phase in equilibrium with the adsorbed phase, and the derivative on the left hand side of the equation is taken at constant adsorption levels, Γ. If we further assume that $V^{(a)} \ll V^{(g)}$ and the ideal

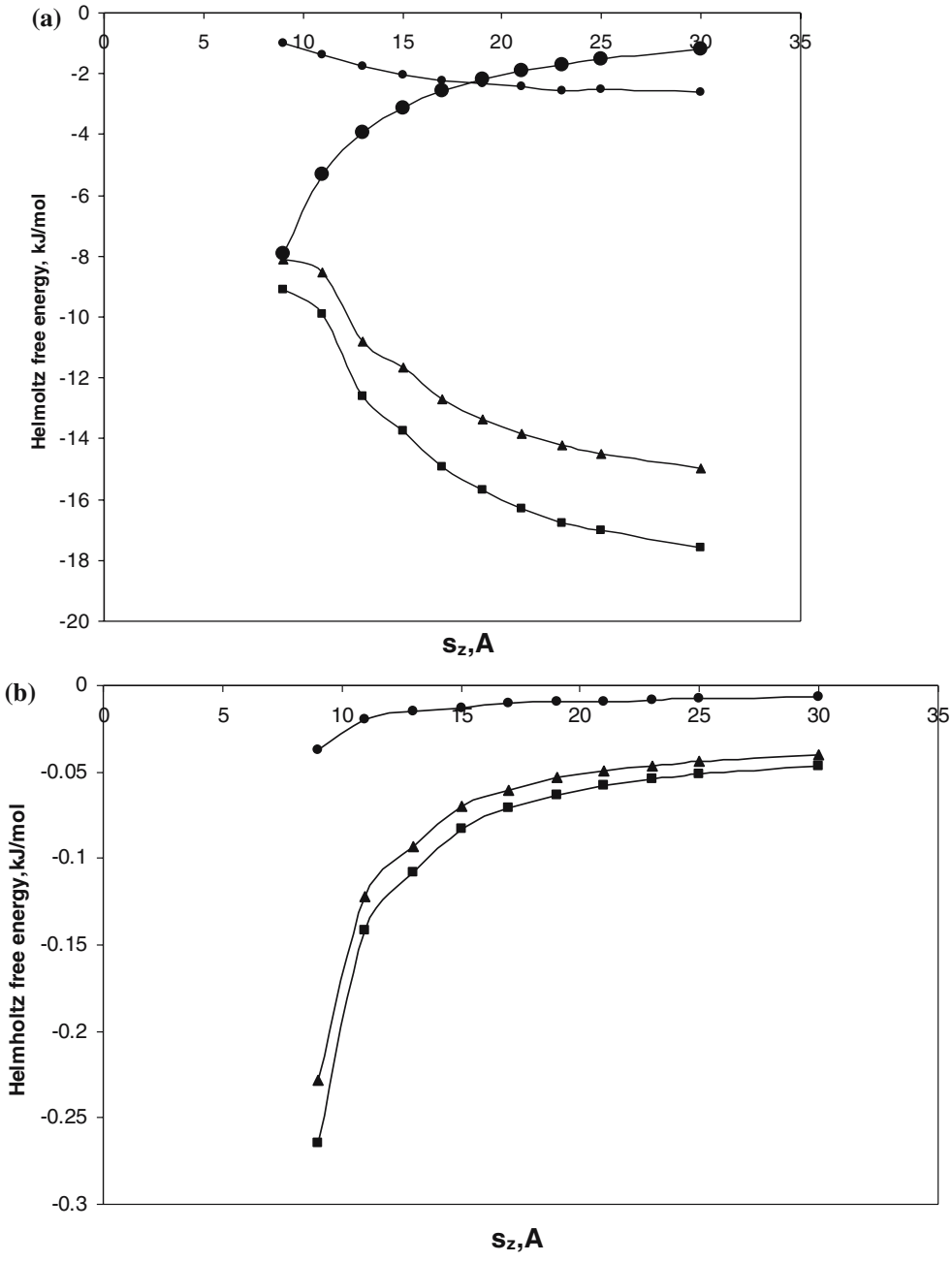

Figure 5. (a) Fluid–wall (●), fluid–fluid electrostatic (▲), fluid–fluid dispersion (•) and total fluid–fluid, dispersion + electrostatic (■) interaction energy as a function of pore sizes at 3.1 kpa, 298 K and $\varepsilon_{fw} = 0.66$ kJ/mol. The fluid is liquid-like at these conditions. (b) Fluid–fluid electrostatic (▲), fluid–fluid dispersion (●) and total fluid–fluid, dispersion + electrostatic (■) interaction energy as a function of pore sizes at 0.7 kpa, 298 K and $\varepsilon_{fw} = 0.66$ kJ/mol. The fluid is vapor-like at these conditions.

gas law holds for the coexisting gas phase so that $V^{(g)} - V^{(a)} \approx RT/P$ then, with this approximation, and combining equations (53) and (54), we have [8]:

$$\left(\frac{\mathrm{d}\ln P}{\mathrm{d}T}\right)_{\Gamma,A,H} = \frac{q_{st}}{RT^2}. \tag{55}$$

Over small temperature intervals it is usually possible to neglect the temperature dependence of q_{st} so that equation (55) can be integrated to give:

$$(\ln P)_{\Gamma} = \left(\frac{-q_{st}}{RT}\right) + \text{ constant}. \tag{56}$$

We used equation (56) to calculate the isosteric heat of adsorption. Figure 6(a) shows the isosteric heat of adsorption at different pore sizes at low surface coverage, i.e., the number of adsorbed molecules per square nanometer of pore surface. The results in figure 6(a) show that the heat of adsorption increases linearly, but modestly, with surface coverage, which is attributed to increased fluid–wall interactions. The results in figure 6(b) show the heat of adsorption at somewhat higher loadings where fluid–fluid interactions are more important than fluid–wall interactions. At high loadings, the heat of adsorption increases as pore size increases from 11 to 35 Å, because of increased hydrogen bonding between water molecules, although on the vertical scale the differences are modest.

3.3. Comparison with the results of Monte–Carlo simulations (Striolo et al. [10])

The simulated isotherms for 10, 16, and 20 Å slit-pores are compared with results of Striolo et al. [10] in figure 7. The simulation results are noted to be quite close in agreement with the Monte–Carlo simulations, both in the transition pressures and the loadings at higher pressures. The small deviations in pore densities after the transition pressure might be due to the approximation of the RDFs. The simulated pore densities before pore filling are in excellent agreement with the Monte–Carlo simulation results presented in [10], because the RDF values used were more accurate for water vapor.

Figure 8 shows the comparisons of the simulated isosteric heats of adsorption at low coverages, which are in excellent agreement with Striolo's Monte–Carlo results. Deviations were observed in the predicted isosteric heats of adsorption at high coverages, shown in figure 9, and might be attributed to the approximation of RDFs at higher densities.

4. Conclusions

The perturbation theory proposed by Schoen and Diestler [5] was extended by including the electrostatic interactions in the configuration integral. The

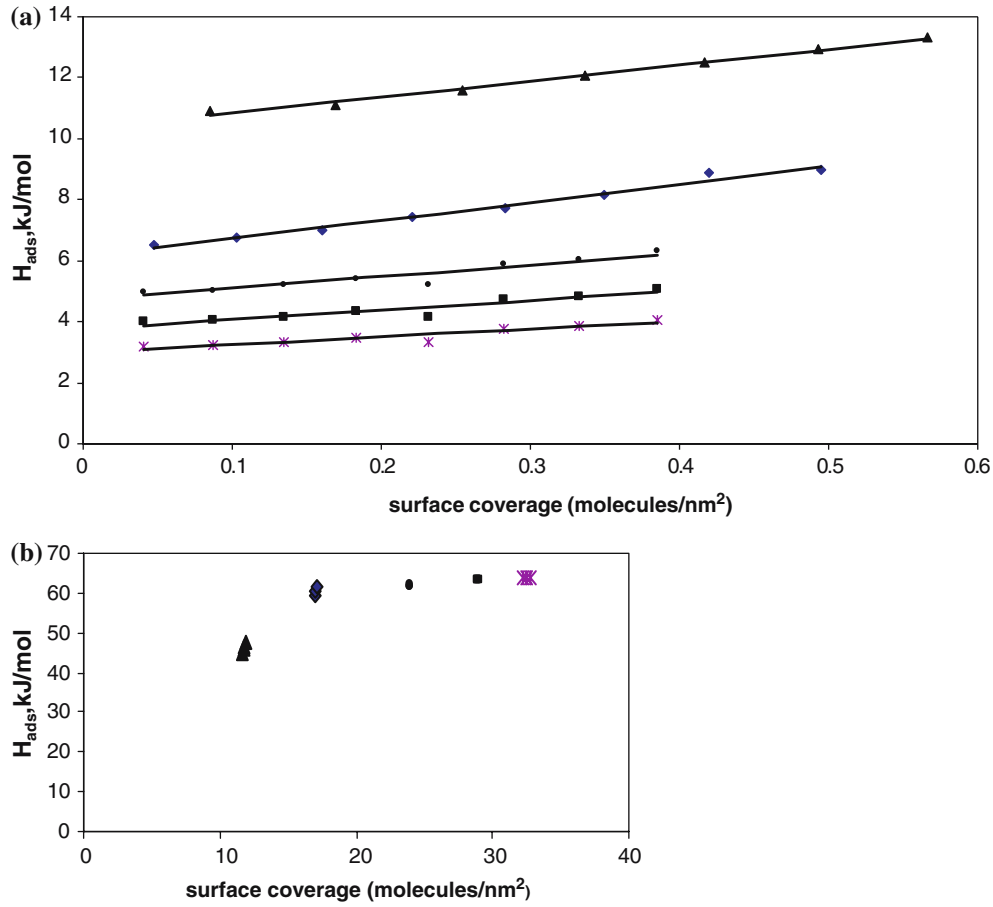

Figure 6. (a) Isosteric heat of adsorption at low surface coverage (number of water molecules adsorbed per nm^2 of pore surface) for pore width of 11 (▲), 15 (♦), 20 (●), 25 (■) and 30 (×) Å. (b) Isosteric heat of adsorption at high surface coverage (number of water molecules adsorbed per nm^2 of pore surface) for pore width of 11 (▲), 15 (♦), 20 (●), 25 (■), and 30 (×) Å.

angular orientation-dependent electrostatic intermolecular potential was approximated by averaging it over all molecular orientations. This change enabled the model to simulate the thermodynamic properties of polar molecules confined in the nanoporous materials. The simulated isotherms and isosteric heats of adsorption of water in nanoslit-pores are in good agreement with the results obtained by Striolo et al. [10] using Monte–Carlo simulations.

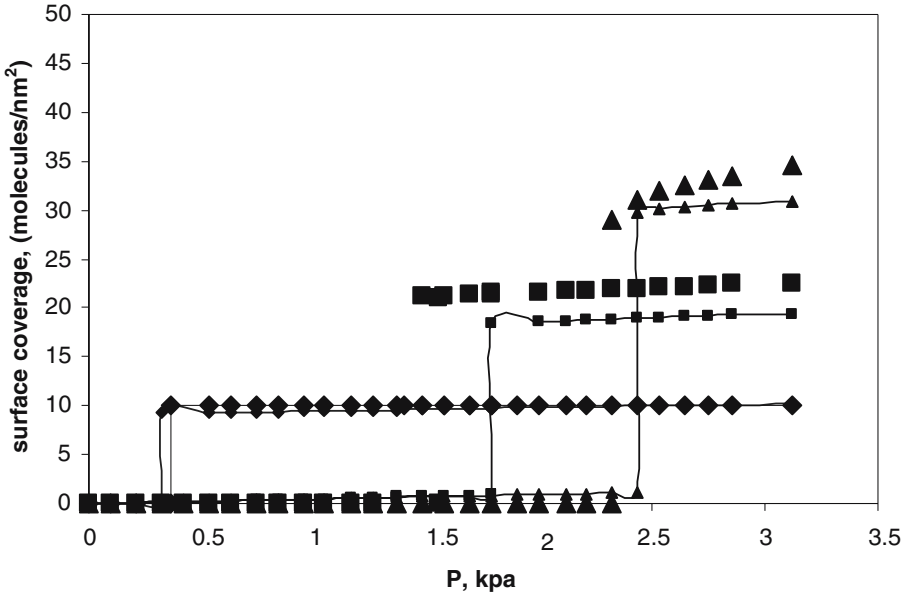

Figure 7. Comparison of simulated surface coverage as a function of bulk pressure (small symbols) with the results of Striolo et al. [10] (large symbols) for pore sizes of 10 (♦), 16 (■), and 20 (▲) Å at 298 K and $\varepsilon_{fw} = 0.336$ kJ/mol.

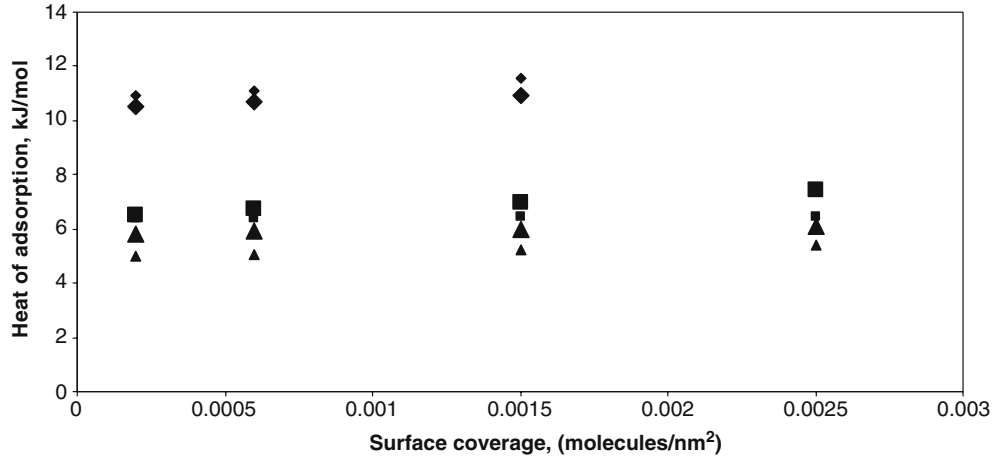

Figure 8. Comparison of simulated heat of adsorption as a function of low surface coverage (small symbols) with the results of Striolo et al. [10] (large symbols) for pore sizes of 10 (♦), 16 (■), and 20 (▲) Å at 298 K and $\varepsilon_{fw} = 0.336$ kJ/mol.

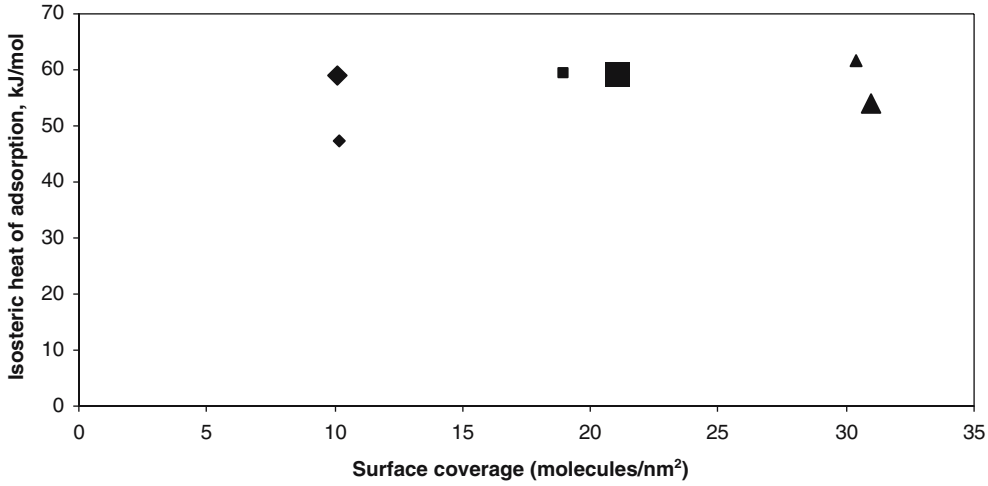

Figure 9. Comparision of simulated heat of adsorption as a function of high surface coverage (small symbols) with the results of Striolo et al. [10] (large symbols) for pore sizes of 10 (♦), 16 (■), and 20 (▲) Å at 298 K and $\varepsilon_{fw} = 0.336$ kJ/mol.

References

[1] M. Rigby, E. B. Smith, W. A. Wakeham and G. C. Maitland, *The Forces Between Molecules* (Clarendon Press, oxford,1986).
[2] D. A. McQuairrie, *Statistical Mechanics* (Harper & Row, New York, 1976).
[3] T. M. Reed and K. E. Gubbins, *Applied Statistical Mechanics* (Mc-Graw Hill, NewYork, 1973).
[4] C. G. Gray and K. E. Gubbins, *Theory of Molecular Fluids,Vol.1: Fundamentals* (Clarendon Press, Oxford 1984).
[5] M. Schoen and D. J. Diestler, J. Chem. Phys. 109 (1998). 5596.
[6] S. Jiang, C. L. Rhykerd and K. E. Gubbins, Mol. Phys. 79 (1993) 373.
[7] R. Evan, U. M. B. Marconi and P.Tarazona, Chem. Soc. Farad. Trans. 2, 82 (1986) 1763.
[8] P. B. Balbuena and K. E. Gubbins, Langmuir, 9 (1993) 1801.
[9] Z. Tan and K. E. Gubbins, J. Phys. Chem. 94 (1990) 6061.
[10] A. Striolo, A. A. Chialvo, P. T. Cummings and K.E.Gubbins, Langmuir 19 (2003) 8583.
[11] G. M. Davis and N. A. Seaton, Langmuir 15 (1999) 6263.
[12] T. M. Truskett, P. G. Debenedetti and S. Torquato, J. Chem. Phys.114 (2001) 2401.
[13] T. M. Truskett, P. G. Debenedetti, S. Shastry and S. Torquato, J. Chem. Phys. 111 (1999) 2647.
[14] A. Giaya and R. W. Thompson, J. Chem. Phys. 117 (2002) 3464.
[15] A. Giaya and R.W.Thompson, J. Chem. Phys. 116 (2002) 2565.
[16] J. M. Smith, H. C. Van Ness and M. M. Abbott, *Introduction to Chemical Engineering Thermodynamics, Ch. 3*, 5th ed. (McGraw Hill, New York 1996).
[17] J. M. Prausnitz, R. N. Lichtenthaler and E.Gomes de Azevedo, *Molecular Thermodynamics of Fluid-Phase Equilibria*, 3rd ed. (Prentice-Hall, NJ, 1999).
[18] J. W. Tester and M. Modell, *Thermodynamics and its Applications*, 3rd ed. (Prentice Hall, Engleword Cliffs, NJ 1997).